

Offset dependence of overburden time-shifts from ultrasonic data

Audun Bakk^{1*}, Rune M. Holt², Andreas Bauer^{1,3}, Bastien Dupuy¹
and Anouar Romdhane¹

¹SINTEF, Department of Petroleum, S.P. Andersens veg 15b, 7031 Trondheim, Norway, ²Norwegian University of Science and Technology, Department of Geoscience and Petroleum, S. P. Andersens veg 15a, 7031 Trondheim, Norway, and ³Present address: AkerBP, Munkegata 26, 7011 Trondheim, Norway

Received November 2019, revision accepted April 2020

ABSTRACT

Depletion or injection into a reservoir implies stress changes and strains in the reservoir and its surroundings. This may lead to measurable time-shifts for seismic waves propagating in the subsurface. To better understand the offset dependence of time-shifts in the overburden, we have systematically quantified the time-shifts of three different overburden shales in controlled laboratory tests. These experiments may be viewed as an analogue to the time-shifts recorded from seismic field surveys. For a range of different stress paths, defined as the ratio between the horizontal and the vertical stress changes, the changes of the P-wave velocities in different directions were measured such that the offset dependence of time-shifts for different stress paths could be studied. The time-shifts are stress path dependent, which is particularly pronounced at large offsets. For all stress paths, the time-shifts exhibit a linearly decreasing trend with increasing offset, that is, a negative offset gradient. At zero offset, for which the ray path is normal to the bedding, the time-shifts are similar for all investigated stress paths. The isotropic stress path is associated with the smallest offset gradient of the time-shifts. In contrast, the constant-mean-stress path shows the largest gradient with a flip in the polarity of the time-shifts for the largest offsets. The separate contributions from the strain and velocity changes to the time-shifts were also quantified. The time-shifts for the isotropic stress path are dominated by the contribution from velocity changes at all offsets. In contrast, the strain contributes significantly to the time-shifts at small offsets for the constant-mean-stress path. This shows that the offset dependence in pre-stack seismic data may be a key to understand the changes of subsurface stresses, pore pressure and strain upon depletion or injection. To utilize this knowledge from laboratory experiments, calibrated rock physics models and correlations are needed to constrain the seismic time-shifts and to obtain an adequately updated geological model reflecting the true anisotropic nature of the subsurface. This may have important implications for improved recovery and safety, particularly in mature fields.

Key words: Anisotropy, Rock Physics, Monitoring, Time lapse, Seismics.

1 INTRODUCTION

The petroleum sector has, over the last years, been under pressure to deploy safer and more efficient operations for improved utilization of the resources. During the production the

* E-mail: Audun.Bakk@sintef.no

reservoir depletes, implying significant alterations in the surrounding rocks, manifested as stress, strain and pore pressure changes. Repeated (4D) seismic surveys turn out to be a powerful tool for monitoring these subsurface changes (MacBeth *et al.*, 2019). Since the first studies, showing the sensitivity of seismic time-lapse data to the subsidence and the reservoir compaction in the Valhall Field (Hall *et al.*, 2002) and the Ekofisk Field (Guilbot and Smith, 2002), a vast number of 4D studies have been published. Already in these early studies, it was evident that the entire subsurface was influenced by the depleting reservoir, manifested as seafloor subsidence, and alterations in the overburden (including the cap rock) and the underburden. The contribution from the mechanical changes in the overburden rocks to the two-way travel-time shifts, is often as significant as the contribution from the fluid and porosity changes in the reservoir (Kenter *et al.*, 2004; De Gennaro *et al.*, 2008; Herwanger and Horne, 2009; Hodgson, 2009; Røste and Ke, 2017; MacBeth *et al.*, 2019). The altering overburden is also commonly associated with safety issues such as fracture growth, fault reactivation, leakages and well instabilities. Thus, in addition to the reservoir itself, the overburden as well as the sideburden and underburden are essential components contributing to the ‘whole earth’ 4D effects (Hatchell *et al.*, 2003; Hawkins *et al.*, 2007; Tempone *et al.*, 2009).

A main aspect of 4D seismic monitoring is to enable accurate predictions of strain and stress changes in the overburden of the depleting reservoir. However, such predictions are difficult because of nonlinear elasticity and non-reversible (plastic) effects during rock deformations, complex geology, and fracturing or fault reactivation (Zoback and Zinke, 2002; Angus *et al.*, 2015; Lavrov, 2016; Yuan *et al.*, 2018). In low-permeability overburden rocks, the reservoir depletion also results in pore pressure changes of the overburden. Such pore pressure changes are often ignored, although they may have a crucial impact on the drilling efficiency and the borehole stability during infill drilling (Ditlevsen *et al.*, 2018). The pore pressure changes in the overburden significantly depend on the stress path resulting from the reservoir deformations (Holt *et al.*, 2018) and is expected to affect the 4D seismic signature. A careful analysis of such time-lapse effects may therefore significantly improve the drilling efficiency and recovery in mature fields (e.g. Calvert *et al.*, 2018) and ultimately enable a successful well abandonment.

Travel-time changes of seismic waves are commonly used to quantify the resulting effects of the altering subsurface. For a single, horizontal, homogeneous and isotropic layer, Landrø and Janssen (2002) showed that the strain (compaction

or expansion) may be separated from the velocity changes by comparing near- and far-offset 4D travel-time data. In reality, the subsurface is more complex, often with shales exhibiting anisotropy (Jones and Wang, 1981; Thomsen, 1986). Also, heterogeneities, stress accumulations and fault systems need to be accounted for. This may show up as localized changes of the fractional time-shifts (time-strains; Rickett *et al.*, 2007). The nonlinear dynamic stiffness model proposed by Prioul *et al.* (2004) has been applied in several works to accommodate for both intrinsic and stress-induced anisotropy (e.g. Herwanger *et al.*, 2007; MacBeth *et al.*, 2018).

To resolve the non-uniqueness inherent to inversion of the time-lapse strain and velocity fields, it is often assumed that the normalized vertical P-wave velocity change (ΔV_z) is linearly related to the vertical strain (ε_z). This is commonly termed as the *R*-factor model (Hatchell and Bourne, 2005; Røste *et al.*, 2005):

$$\frac{\Delta V_z}{V_z} \approx R\varepsilon_z, \quad (1)$$

where the ε_z is defined positive for compaction. This model has mostly been used for 4D post-stack seismic analysis (e.g. Hatchell and Bourne, 2005; Røste and Ke, 2017), although it is more and more common to use the relation for 4D pre-stack analysis (which was the original idea of Røste *et al.*, 2005). By acknowledging the anisotropy of the subsurface, one can utilize the full potential of pre-stack seismic data by, for example, including ray-angle dependence of the *R*-factors (e.g. Hawkins, 2008; Rodriguez-Herrera *et al.*, 2015; Kudaraova *et al.*, 2016). Although the *R*-factors are commonly assumed constant for larger stretches of the subsurface, the data from De Gennaro *et al.* (2008) from the Elgin and Franklin fields show that the *R*-factor may vary significantly with depth throughout the overburden.

In this work, we present laboratory experiments on three overburden field cores and describe how the time-shifts are related to offsets and stress paths, which may open new possibilities for improved 4D seismic interpretation. The experiments were performed in a load frame where the horizontal and vertical stresses are changed in different ratios to mimic different stress paths. Simultaneously, ultrasonic P-wave velocities at multiple angles were recorded to quantify their strain and stress sensitivities. We explain how the time-shifts calculated from laboratory data may be compared with the time-shifts of 4D seismic data for an anisotropic subsurface. The expressions and methods are applicable to both overburden and reservoir layers, although we here only discuss it in the context of overburden shales. The strains and velocity changes in the

Table 1 Overview of the tested offshore field cores. TVD: true vertical depth; wt%: weight percent

Shale	TVD (km)	Porosity (%)	Clay content (wt%)	Geological age
1	1.4	36	68	Middle Miocene
2	2.5	29	73	Eocene
3	3.4	24	76	Early Miocene

laboratory data were used to calculate the time-shifts resulting from the stress path variations. After summarizing the experimental results, the strain dependence of the vertical velocity and the offset dependence of time-shifts are discussed.

2 MATERIALS AND METHODS

2.1 Experimental set-up

Three different field shales, preserved as seal peeled cores until testing, were used in the controlled laboratory experiments. One cylindrical sample, 38 mm in diameter and about 60 mm long, from each of the cores was drilled and subsequently stored in Marcol (oil) prior to testing to preserve the natural humidity and saturation. The samples were drilled normal to the visual bedding plane and mounted vertically in a triaxial load frame. All measurements and further analysis assume transverse isotropy with a vertical symmetry axis (VTI). Usually, one refers to the axial direction and the radial plane for laboratory samples. Since the laboratory data are discussed in the context of seismic surveys, we conveniently replace 'axial' and 'radial' with 'vertical' and 'horizontal', respectively. The key characteristics of the different cores are summarized in Table 1. Photos of the shale samples prior to the experiments are provided in Fig. 1.

In the laboratory tests, the samples were initially pre-stressed and exposed to the expected *in situ* brine salinity based upon a pore fluid analysis, whereupon the samples were brought in drained condition to the expected *in situ* stress and pore pressure. Drained condition means that the pore pressure is controlled externally. This procedure is expected to lead to full saturation (Horsrud *et al.*, 1998). A proper saturation and contact between the pore fluid and the external pore pressure transmission fluid was also verified by the measured pore pressure response as expected for saturated shales (Skempton, 1954; Holt *et al.*, 2018).

The tests were performed in a triaxial set-up where the vertical and the horizontal (confining) stresses were adjusted independently, where the horizontal absolute stresses and

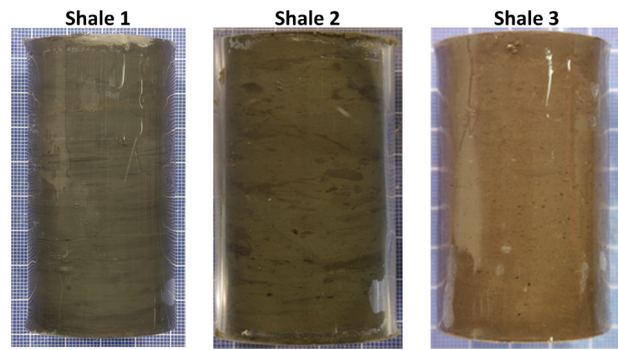


Figure 1 Photos of the three tested field shale samples prior to the testing. After the drilling and trimming, these plugs (cylindrical samples) were wrapped in a shrink sleeve and immediately stored in Marcol (neutral oil) to reduce the possibility for any damage before the laboratory experiments.

stress changes were isotropic in the horizontal plane. This enabled investigation of the stress path dependence of time-shifts. Simultaneously, pulse transmission measurements were acquired providing multidirectional P-wave ultrasonic velocities (cf. Fig. 2). The velocities for the different angles were sampled one-by-one, separated with a small delay (a few seconds) to avoid any noise (interference) from the preceding samplings.

The excitation frequency was 600 kHz for the vertical (0°) P-wave measurement and 500 kHz for the non-vertical (37° , 47° , 68° and 90°) P-wave measurements. The uncertainty in the velocities is estimated from the assessed uncertainties in the picking of arrival times, sample dimensions (length and radius), stresses, strains and temperature fluctuations. The error in the absolute value of the P-wave velocities is estimated to be 1%, where the error in the picking is dominating. The error is defined as two standard deviations, where the 95% confidence interval is equivalent to four standard deviations assuming a normal distribution. However, in this work we only consider the relative changes in the velocities as required for assessing the strain sensitivities (equation (1)) and the time-shifts (equation (5)). An analysis of the relative change in P-wave velocities for a field shale using 50 waveforms, at all the different angles considered here, gave an error of 0.1% relative to the absolute velocity, corresponding to 2–3 m/s. This will then represent the error in picking in this case. The stress and temperature corrections for the relative velocities are negligible compared with the error in picking. Consequently, the total error for the change in the relative velocities is estimated to be 10^{-3} . The relative uncertainties of the horizontal and vertical dimensions (strains) are estimated from a calibration test to be 10^{-4} and 10^{-5} , respectively, which is negligible

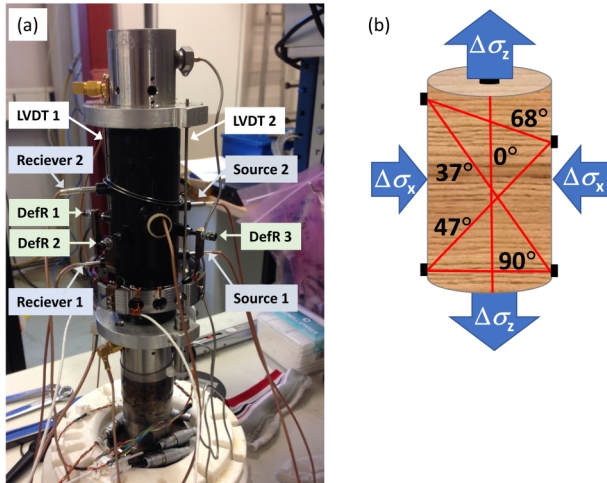


Figure 2 (a) The set-up ('stack') shown with a Viton rubber sleeve surrounding the sample. Source/receiver: two P-wave sources and receivers, respectively, for oblique and horizontal velocity measurements. The transducers for vertical wave propagation are integrated in the front of the load pistons above and beneath the sample, respectively. LVDT: linear variable differential transformers for vertical strain measurements (LVDT 3 is hidden). DefR: attachments for two pairs of cantilevers for horizontal strain measurements (DefR 4 is hidden). (b) At the *in situ* stress and pore pressure, horizontal ($\Delta\sigma_x$) and vertical ($\Delta\sigma_z$) stress changes were applied to the cylindrical field shale samples to obtain the different stress paths as illustrated in Fig. 3. The stresses are isotropic in the horizontal plane. Simultaneously, ultrasonic velocities were measured along the ray paths (red lines) in multiple directions (0° , 37° , 47° , 68° and 90°) that were constrained by the positions of the transducers (black discs).

compared with the error in the relative velocities. Thus, the resulting errors of the R -factors and the time-shifts (prior NMO correction) are both estimated to be 10^{-3} , since the dominating error in both these quantities is associated with the change in the relative velocity (cf. equations (1) and (5), respectively). The error is visualized in the plots with error bars covering the 95% confidence interval. Moreover, for the oblique ultrasonic measurements, we use very small transducers (2 mm in diameter), which in practice provide a direct quantification of the group velocities as verified from finite-difference wave-propagation simulations. The group velocities were then conveniently converted to the corresponding phase velocities for the given anisotropy (Thomsen, 1986). The determination of the C_{13} dynamic (VTI) constant was optimized by including all the oblique P-wave measurements in the inversion for this constant, in addition to the principal P-wave velocities and the vertical S-wave velocity. This significantly improves the determination of the C_{13} (or alternatively Thomsen's δ parameter)

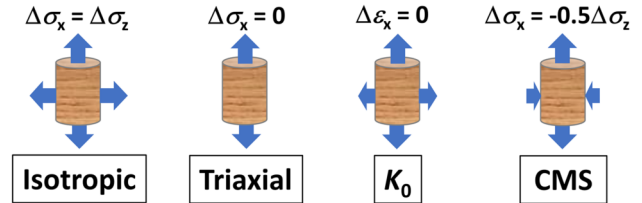


Figure 3 The applied *in situ* stress paths on the field samples where $\Delta\sigma_z$ is the vertical stress change, $\Delta\sigma_x$ is the horizontal stress change, and ϵ_x is the horizontal strain. Isotropic: isotropic stress change; triaxial: uniaxial (vertical) stress change; K_0 : stress change constrained by zero horizontal strain; CMS: constant-mean-stress change. The arrows indicate the magnitude and direction (polarity) of the stress changes, where arrows pointing out of the sample represent a stress decrease and arrows pointing towards the sample represent a stress increase. Here we illustrate the second part of each stress cycle with 5 MPa vertical stress decrease (see Fig. 4). In the first part of each stress cycle, the polarity of the stress changes is inverted (5 MPa vertical stress increase).

as compared with having only one oblique angle (e.g. Hornby, 1998).

The vertical strain was determined as the average value of recordings from three linear variable differential transformers (LVDTs) separated by 120° azimuthally (cf. Fig. 2a). Similarly, the horizontal strains were determined as the average values of recordings from two orthogonal pairs of cantilevers located in the same horizontal plane (exactly in the middle between ultrasonic receivers 1 and 2). The cantilevers' attachments are rotated 45° azimuthally relative to the vertical plane of the ultrasonic transducers and consist of pins penetrating the sleeve ensuring direct contact with the sample. There is no indication of (close to) rock failure behaviour in any of the tests. Furthermore, we assume that the deformations are homogeneous throughout the sample, which mechanically is reflected in similar (parallel) response of the individual strain measurements in the vertical and horizontal directions, respectively. The tests follow the standard guidelines of geomechanical tests (Dudley *et al.*, 2016). Aluminium and polyetheretherketone (PEEK) standards are used for the static and dynamic calibration of the set-up.

2.2 Stress paths

When the sample reached the estimated *in situ* stress and pore pressure after proper consolidation, we applied a sequence of undrained stress variations (cycles) with different stress paths as illustrated in Fig. 3: (1) isotropic stress change (isotropic), (2) uniaxial (vertical) stress change (triaxial), (3) stress change constrained by zero horizontal strain (K_0) and

Table 2 *In situ* stress paths and their corresponding value of κ defined in equation (2). The κ value for the K_0 stress path varies as it depends on the specific shale's properties

Stress path	κ (-)	Description
CMS	-0.5	Constant-mean-stress change
Triaxial	0	Uniaxial stress change
K_0	0.65–0.76	Horizontal stress change constrained by zero horizontal strain
Isotropic	1	Isotropic stress change

(4) constant-mean-stress change (CMS). Undrained conditions mean that the pore fluid is not allowed to flow in and out of the sample, except for a tiny dead volume of 2 ml in our set-up. This means that there is no external control of the pore pressure, although the pore pressure is continuously monitored. The undrained state is assumed to be the most realistic condition for the overburden within a typical time span of a petroleum production case, as a result of the low permeability of shales (Horsrud *et al.*, 1998). For the systematic analysis of the different stress variations, it is convenient to introduce a stress path parameter, κ , which describes the change in the horizontal stress ($\Delta\sigma_x$) relative to the vertical stress ($\Delta\sigma_z$) (Holt, 2016):

$$\kappa \equiv \frac{\Delta\sigma_x}{\Delta\sigma_z}. \quad (2)$$

An overview of the different stress paths and the corresponding values of the κ is summarized in Table 2.

For each *in situ* stress path cycle, we initially changed the vertical stress by 5 MPa while the horizontal stress was changed according to the specific stress path (see Table 2). The magnitude of the stress changes expected for the overburden above a depleting reservoir will however depend on many factors, such as the reservoir shape, depth and depletion; elastic contrast between the reservoir and surroundings and the layering (stress arching); and proximity to the reservoir (Hawkins *et al.*, 2006; Herwanger and Horne, 2009; Morita and Fuh, 2009; Toomey *et al.*, 2017). This may result in smaller or larger stress changes where 5 MPa may be representative for some field scenarios. After each stress step, there was a hold period to let the sample consolidate (pore pressure equilibration), which typically took 2–4 hours. This relatively fast consolidation for the shales was possible since the samples were in an undrained state and that the dead volume was small as compared with the pore volume of the samples (pore volume is typically around 20 ml for a sample with 30% porosity). After the consolidation upon the vertical stress increase, we measured the quantities used for the determina-

tion of the static and the dynamic properties (averaged over several data points). After this, we stepped down to the *in situ* stress and obtained a new set of static and dynamic quantities after the consolidation. The total sequence consisting of (1) vertical stress increase, (2) consolidation, (3) vertical stress decrease and (4) consolidation, where the horizontal stress was simultaneously changed according to equation (2) in all steps, is termed as one stress cycle. Each stress cycle for each specific stress path was repeated once for Shale 1 and 3, giving four sets of changed dynamic and static quantities (P-wave velocity changes and strains) for each stress path. For Shale 2, only the isotropic stress path was repeated. In this work, we did not observe large deviations of the absolute values of these data between the different loading and unloading steps, and the resulting time-shifts are simply averaged for each stress path. In general, the (undrained) pore pressure was close to the initial *in situ* value after the end of each cycle (typically 0.1–0.4 MPa above *in situ* pore pressure). This pattern was also seen for the strain, which is a good indication of proper consolidation and near elastic behaviour. However, to exclude any global drift in the pore pressure, the sample was drained to *in situ* pore pressure prior each new cycle (Fig. 4).

2.3 Time-shifts

The P-wave group velocities were determined in multiple directions (ray angles) ranging from 0° to 90° with respect to the bedding normal (Fig. 2). The similarities between the laboratory test and a typical seismic survey are illustrated in Fig. 5 assuming straight ray paths propagating in a homogeneous rock. In the seismic case, this implies that the incident ray path is (partially) reflected because of impedance contrast between the single homogeneous layer of propagation we consider here and the layer beneath. The time from the source to the receiver is termed the two-way travel-time in seismics. In the laboratory test, we do not consider reflections, only pulse transmissions. When considering seismic time-shifts, the reflections themselves have no influence on the velocities nor the

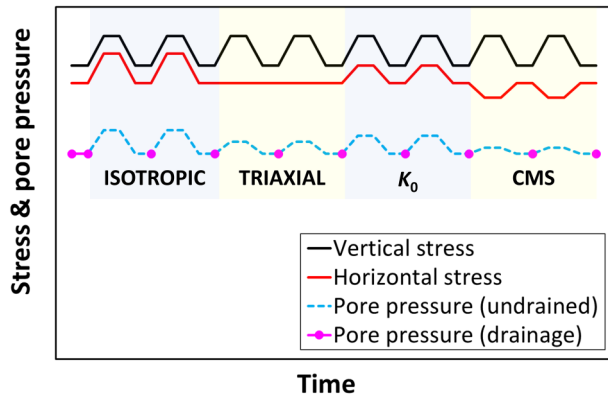


Figure 4 Schematic illustration of the test protocol with the different *in situ* stress path cycles. The pore pressure was drained to the *in situ* value prior to each cycle to avoid drift in the test conditions. During the stress cycles, the pore pressure was kept undrained where the actual pore pressure response depends upon the specific material properties (the broken line for the undrained pore response is only indicative).

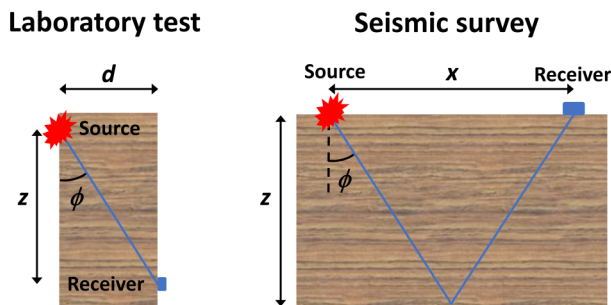


Figure 5 A laboratory test may be regarded as an analogue to a reflection seismic survey. The ϕ is the ray (group) angle; z is the vertical separation between the source and receiver; and d and x are the horizontal separation between the source and receiver in the laboratory sample and in the field case, respectively.

velocity changes. Thus, a reflected wave in a single homogeneous layer has the same travel-time as a directly transmitted (not reflected) wave when the total path lengths are equivalent in the two cases. The latter also underline the similarity between the reflected waves in seismic surveys and the direct waves in the laboratory experiment with respect to time-shifts, as the angle dependence of time-shifts observed in the laboratory can be linked to offset dependence of reflected waves in the subsurface (cf. Fig. 5). The heavy-damping Viton rubber sleeve, which is confining the samples in the laboratory tests, together with the low-impedance (relative to the samples) confining fluid rules out the possibility for faster surface waves interfering with the first arrival of the P-waves. Moreover, the field samples are relatively homogeneous on the length scale of

the wavelength (4–5 mm), implying no bending of the waves. Thus, since the P-waves are the fastest waves, the first arrivals will in our set-up provide the true P-wave velocities by considering the shortest distance between the source and the receiver. This also rules out the possibility for interference between the direct P-wave arrival and (multiple) wave reflections from the sample's boundaries. The consistency in the wave picking is clearly visible in the recorded waveforms for Shale 2 (cf. Fig. 6). This was also verified with finite-difference simulations of the wave propagation with the experimental set-up utilized in these tests, and with the calibration tests. The waveforms for the vertical (0°) P-wave at the initial *in situ* and the CMS stress states are also provided. These two recordings are separated by 75 hours in the test, which demonstrates the repeatability in the waveforms and the quality of the first arrival. To further support the quality of the picking of the first arrivals (considering the first extremum of the waveform), a spectral ratio analysis was done. This analysis, which was limited to the first wavelet, shows that the corresponding centre (dominating) frequency is changing by less than 10 Hz during the whole timespan of the *in situ* stress variations we have considered in this work. Such changes are very small when compared with the 0.5–0.6 MHz source. Moreover, the damping of the signal between the *in situ* stress level and the different stress stages shows no distinct trend and is not significant in magnitude (less than 0.1 dB/cm). This suggests that the picking of the first extremum is not influenced by the stress state for the different *in situ* stress variations and is not adding any significant errors beyond what is already discussed in Section 2.1.

The analogue to the two-way travel-time in seismic is defined in the laboratory test as two times the measured travel-time from the source to the receiver. Furthermore, we can define an offset in the laboratory test ($2d \rightarrow x$ in Fig. 5) such that the idealized physical models in the lab and in the field can also be treated equally mathematically. The Pythagorean equation gives the two-way travel-time, t , which is valid for any anisotropy (Thomsen, 1986):

$$t^2 = \frac{4z^2 + x^2}{V^2(\phi)} = \left(\frac{V_z}{V(\phi)} \right)^2 \left(t_z^2 + \frac{x^2}{V_z^2} \right), \quad (3)$$

where V_z is the vertical group velocity, t_z is the vertical two-way travel-time time and $V(\phi)$ is the group velocity at ray angle ϕ . In the 4D case, we assume small changes in thickness (Δz) and velocities ($\Delta V(\phi)$):

$$\frac{\Delta z}{z}, \frac{\Delta V(\phi)}{V(\phi)} \ll 1. \quad (4)$$

The first-order differentials of equation (3) with respect to Δz and $\Delta V(\phi)$ at ray angle ϕ yield the relative time-shift at

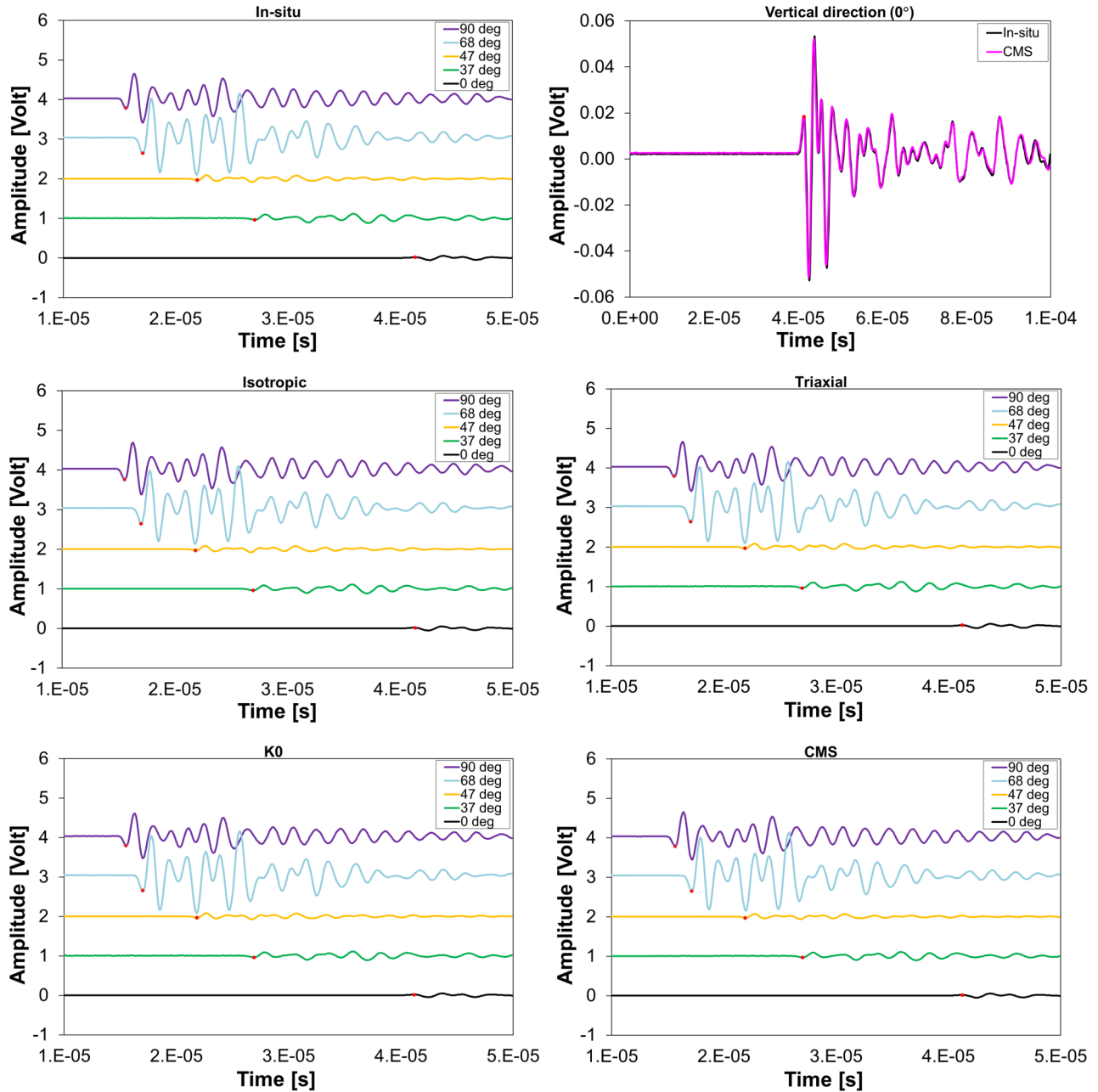


Figure 6 Recorded waveforms for the P-wave signals for Shale 2 obtained at *in situ* stress conditions prior to the first isotropic loading–unloading cycle ('In-situ'), and at the end of consolidation at the first stress change (vertical stress increase) for the isotropic, triaxial, K_0 and CMS stress paths (cf. Table 2). The quality and repeatability of these waveforms are representative for the other waveforms for this shale and the waveforms of the two other shales discussed in this work. The picked arrivals, considering the first extremum of the waveform, are indicated with red dots for the different propagation directions (e.g. '0 deg' corresponds to vertical P-waves). The waveforms for the vertical P-wave at the initial *in situ* state and the CMS (vertically stressed) state are also provided to demonstrate the repeatability in the waveforms and the quality of the first arrival ('Vertical direction (0°)').

a given offset with ray angle ϕ :

$$\begin{aligned} \frac{\Delta t}{t} &\equiv \frac{t_{\text{repeat}} - t_{\text{baseline}}}{t_{\text{baseline}}} \approx \frac{\Delta z}{z} \left(\frac{2z}{tV(\phi)} \right)^2 - \frac{\Delta V(\phi)}{V(\phi)} \\ &= -\varepsilon_z \cos^2 \phi - \frac{\Delta V(\phi)}{V(\phi)}, \end{aligned} \quad (5)$$

where the vertical strain (ε_z) is defined positive for compaction ($\Delta z < 0$):

$$\varepsilon_z \equiv -\frac{\Delta z}{z}. \quad (6)$$

Equation (5) is the anisotropic version of the relative time-shift expression proposed by Landrø and Janssen (2002). In the anisotropic case, both the velocity and the velocity changes depend upon the ray angle in contrast to the isotropic case. Even though the strain not explicitly appears in the velocity term of equation (5), we will show in Section 3 that the velocity changes also are strain- and stress path dependent. As we only consider the homogeneous single-layer case here, the relative time-shift in equation (5) is equivalent to the time-strain (Hodgson, 2009).

Since much of the seismic data used for conventional time-lapse analysis are post-stack, the corresponding normal-moveout (NMO)-corrected two-way travel-time shift in the anisotropic case may also be of interest. We follow the procedure applied by Landrø and Stammeijer (2004) for the isotropic case and generalize this to the anisotropic case. A simple expansion and factorization of the relative time-shift yield

$$\frac{\Delta t}{t} = \frac{\Delta t}{\Delta t_z} \frac{t_z}{t} \frac{\Delta t_z}{t_z}, \quad (7)$$

where the quantities are defined in relation to equations (3) and (5). The NMO stretch of the travel-time shift for the constant velocity case, now with anisotropy, is obtained by taking the first-order differential of equation (3) with respect to Δt_z :

$$\frac{\Delta t}{\Delta t_z} = \frac{t_z V_z^2}{t V^2(\phi)} = \frac{t}{t_z} \cos^2 \phi. \quad (8)$$

By inserting equation (8) into equation (7) and then replacing the left side of equation (5) by equation (7), the relative NMO-corrected travel-time shift in the anisotropic case after some rearrangements becomes

$$\left. \frac{\Delta t_z}{t_z} \right|_{\text{NMO}} = -\varepsilon_z - (1 + \tan^2 \phi) \frac{\Delta V(\phi)}{V(\phi)}, \quad (9)$$

where the velocity term is proportional to the relative velocity change along the ray path modified with an angularly

dependent prefactor, in contrast to the isotropic case (Landrø and Stammeijer, 2004).

In the laboratory tests, contrary to the field case, the offset is not constant as the non-vertically oriented transducers are attached to the sample's circumference and moves according to the horizontal strain. Thus, to tie the lab data to the 4D seismic case where discrete (fixed) offsets are considered, we need to compensate for a slightly different group angle ($\Delta\phi$) associated with the horizontal movement of the transducers that will influence the $\Delta V(\phi)$ in equation (5). By using a simple geometric consideration, it can be shown that this correction can be approximated by

$$\Delta\phi \approx -\frac{\varepsilon_x}{2} \sin(2\phi), \quad (10)$$

where ε_x is the horizontal strain. The angular correction scales linearly with the horizontal strain, which is largest for the CMS stress path in our case and vanishes at 0° and 90° as a result of the sine term. The angular correction in equation (10) implies a minor correction of the measured relative time-shift of maximum 10^{-5} for the present data set.

The relative time-shifts discussed here are estimated from the laboratory data of the vertical strains and the multidirectional wave velocity changes by the use of equation (5), including the correction of the ray angle from equation (10). Thus, we may in principle compare our estimated time-shifts with the time-shifts obtained from 4D seismic reflection data at different (fixed) offsets represented by angle-band stacks. In our data, there are no big differences in the absolute values of the travel-time-shifts associated with the loading (stress increase) step and the unloading (stress decrease) step. Thus, the time-shifts discussed here are the average of the absolute values for each stress path. The polarity of the presented time-shifts is conveniently tied to unloading of the vertical stress, and consequently the polarity of the time-shift for the vertical-loading cases is simply inverted to represent an unloading scenario, which is typical for the overburden above a depleting reservoir.

3 RESULTS AND DISCUSSION

3.1 Strain sensitivities of vertical P-wave velocities

It has been known for a long time that stress changes and deformations of porous rocks imply variations of wave velocities. This is commonly termed stress or strain sensitivity of velocities. An implication of this is that the dynamic stress-strain relation becomes nonlinear (e.g. Thurston and Brugger, 1964; Johnson and Rasolofosaon, 1996; Prioul *et al.*, 2004;

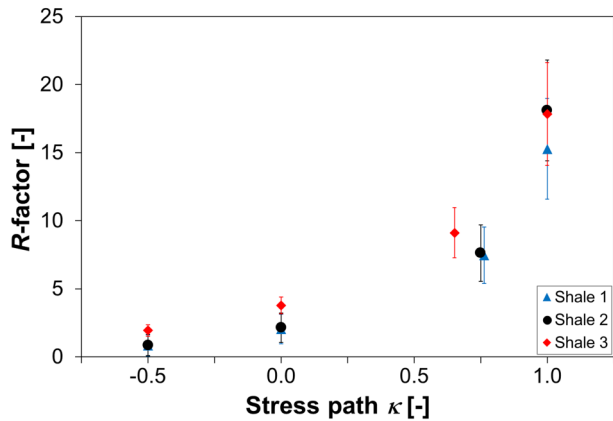


Figure 7 Strain sensitivity of the vertical ultrasonic P-wave velocity (R -factor; cf. equation (1)) measured normal to the bedding plane, versus the stress path parameter, κ , as defined in equation (2) and quantified in Table 2. The data are obtained with 5 MPa vertical stress changes as the average values of all loading and the unloading steps for the specific stress path. The error bars correspond to the 95% confidence interval.

Fuck and Tsvankin, 2009). Consequently, the depletion of a hydrocarbon reservoir leads to a spatially varying stress-induced dynamic anisotropy of the entire subsurface. This is true irrespective of the heterogeneity and symmetry of the baseline velocity field, the symmetry of the static stiffness and the geometry of the reservoir (Fuck *et al.*, 2009). Several laboratory experiments show that both the reservoir rocks and the overburden rocks exhibit significant stress and strain sensitivities (e.g. Dillen *et al.*, 1999; Pervukhina *et al.*, 2008; Holt *et al.*, 2011; Sarout *et al.*, 2014).

For the shales investigated here, the estimated R -factors show a strong and nonlinear dependence on the stress path, with a rapid increase with decreasing shear stress as shown in Fig. 7. A significant stress path dependence of the R -factor is also valid in the case of negligible stress path dependence on the stress sensitivity of the vertical P-wave velocity, since the vertical strain is stress path sensitive itself (Holt *et al.*, 2018). Thus, the velocity term of the time-shift in equation (5) is expected to be significantly influenced by the variety of stress paths along the ray path of investigation. Additionally, the absolute stress level, rock composition and texture (Bathija *et al.*, 2009), and the amplitude of the stress change (Lozovyi *et al.*, 2018) will influence the strain sensitivity. Consequently, as a result of both rock and stress heterogeneity, the R -factor varies spatially (De Gennaro *et al.*, 2008; Røste *et al.*, 2015), which implies potentially large variations of the time-strains.

3.2 Time-shifts from laboratory data

The laboratory experiments discussed here may be viewed as an analogue (physical simulation) to an idealized seismic time-lapse survey with a single layer (cf. Section 2.3). In both cases, compressional waves travel through the rocks in multiple directions, for which altered stresses, strains and pore pressures result in changed velocities; all factors that contribute to the measured travel-time shifts. A major benefit with the laboratory experiments is the explicit measures of all these quantities studied for a range of stress paths and offsets under controlled conditions. Clearly, the high angles that can be achieved in the laboratory (including the 90°) are not normally reached in seismic surveys. Nevertheless, the data are shown to be able to assess the full range.

Figure 8 shows the relative time-shifts for the different ray angles and stress paths. The three different shales exhibit qualitatively very similar trends. Linear trend-lines are inserted to ease the separation between the different stress paths. This should not be interpreted as a ‘linear model’ for the time-shift trends, just a tool to discriminate the main trends for the different stress paths. A more detailed offset analysis would require more data or the implementation of higher order nonlinear dynamic models. The travel-time shifts are largest and almost equal among the different stress paths at zero offset (0°), that is, for the vertical P-waves propagating normal to the bedding. The relative time-shifts decrease for increasing angle (negative gradient), and the gradient is steepest for the constant-mean-stress path. Similar trends are also manifested for the average values of all three shales (cf. Fig. 8). This implies potentially a clear separation between the time-shifts of the different stress paths at larger angles. A complementary manifestation of this is seen in Fig. 9 where the mean relative time-shifts are plotted against the stress path for the distinct ray angles. Clearly, the time-shift dependence on the stress path increases with increasing ray angle. Generally, the time-shifts for the isotropic and the K_0 stress paths behave in a similar way, which is reasonable given the small differences in the stress path parameter κ in Table 2.

The experimental data address the deviating results on the offset trend of time-shifts reported from 4D seismic inversion (MacBeth *et al.*, 2018). Some of these results are based on normal-moveout (NMO)-corrected data (e.g. Landrø and Stammeijer, 2004; Herwanger and Horne, 2009; Kudarova *et al.*, 2016) while other works report pure time-shifts without any NMO correction (e.g. Hawkins, 2008). Obviously, any moveout will imply a huge qualitative and quantitative change in the offset trends of the time-shifts. Because of the

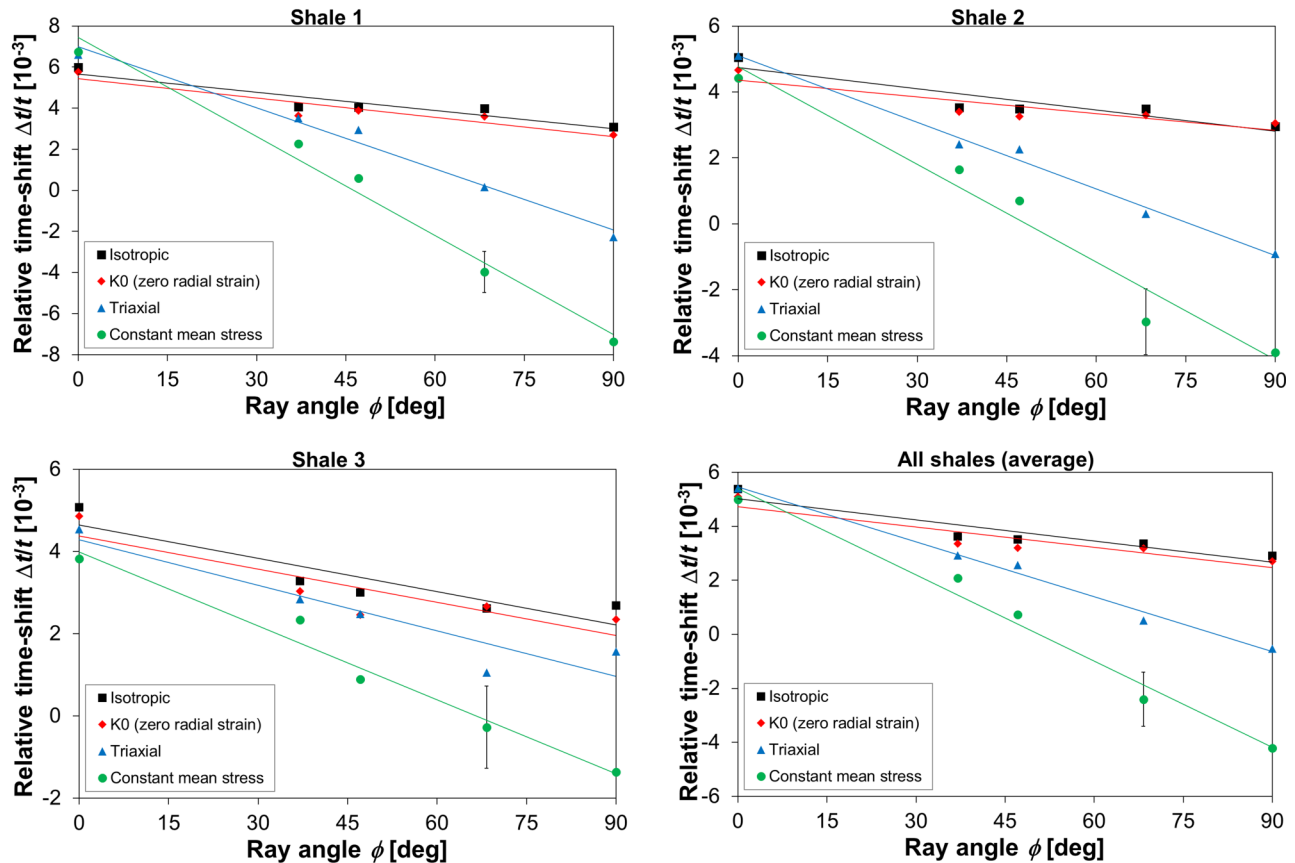


Figure 8 Relative time-shift versus the ray angle for the different stress paths (cf. Table 2) and shales (cf. Table 1) corresponding to 5 MPa vertical unloading. The average values for the three shales are also shown ('All shales (average)'). Linear trend-lines are inserted for each stress path. The error bars correspond to the 95% confidence interval (valid for all data points in the same figure).

intrinsic anisotropy of rocks, the moveout will be nonhyperbolic, even in the single-layer, homogeneous and flat reflector analogue (Grechka and Tsvankin, 1998). In our tests, the complete VTI dynamic and static stiffnesses are obtained. Thus, there is no need for approximated moveout corrections since the anisotropy is *a priori* quantified. The effect of the NMO correction in equation (9) with a constant velocity moveout is shown for the averaged time-shifts in Fig. 10. The NMO is amplifying the stress path separation of the time-shifts at large offsets. This may look appealing, but one should note that the NMO corrections are inevitably accompanied with a corresponding amplification of the error with increasing offset (scales with the factor $(1 + \tan^2\phi)$; cf. equation (9)). Consequently, the gradients of the time-shifts are qualitatively and quantitatively affected when compared with the time-shifts prior to the NMO correction (Fig. 8). With the NMO correction, the time-shifts associated with the isotropic and K_0 stress paths are non-linearly increasing with offset, while for

the CMS stress path the time-shift is non-linearly decreasing with offset. The NMO-stretch flattens out the offset gradient for the triaxial stress path of these shales. In contrast, the time-shifts without NMO correction are linearly decreasing for all stress paths.

The time-shift in equation (5) consists of two terms. One term is explicitly related to the vertical strain and the other term is related to the change in the relative velocity. Since this equation is tied to a 4D field situation at fixed offsets, there will be no explicit geometric contribution from the horizontal strain to the time-shift. However, the horizontal strain together with the vertical strain plays implicitly a crucial role with respect to the velocities, since the strain sensitivities of the velocities are significant and stress path dependent (cf. Fig. 7). The geometric contribution from the vertical strain to the time-shift is visualized for Shale 2 in Fig. 11(a), which is largest for zero offset and diminishes for large offsets as expected as a result of the $\cos^2\phi$ factor in equation (5). The

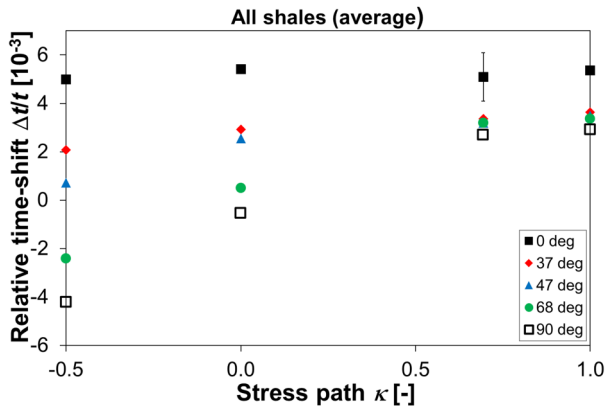


Figure 9 Relative time-shift versus stress path for the different ray angles corresponding to 5 MPa vertical unloading. The data are the average values of the three shales. The error bar corresponds to the 95% confidence interval (valid for all data points).

vertical strain is largest for the constant-mean-stress path, implying the largest geometric contribution on the time-shift for a given offset (cf. Fig. 11b). The geometric contributions to the time-shift for the isotropic and the K_0 stress paths are very small, reflecting the relatively small strains. This emphasizes the importance of a proper assessment of the anisotropic stress-induced sensitivity of the velocities, and its stress path dependence.

3.3 Discussion

The stress-path-dependent travel-time gradients (Figs 8 and 9) may be used to gain very important quantitative and qualitative information about the subsurface, such as stress and pore pressure changes, depletion-induced reactivation of faults and undepleted pockets in the reservoir. The key is to establish a link between the stress changes (stress amplitudes and stress paths) and the velocity changes, which enables to update geomechanical models with a proper separation of strains and velocity changes. This requires integration of an appropriate calibrated rock physics model into the inversion procedure accounting for the intrinsic static and dynamic anisotropy of rocks, in addition to the stress-induced dynamic anisotropy. To adequately account for the heterogeneous changes in a 4D seismic analysis, implying a field-specific stress path field, geomechanical modelling is required accounting for the site's production history, and the geometry and properties of the layers. A geomechanical model that is coupled to a rock physics model converts strains to velocity changes, and thereby the estimated time-shifts can be compared with the time-shifts

derived from the 4D seismic data analysis. To illustrate the potentially wide variety in subsurface stress paths – consider the overburden above a depleting reservoir where a vertical stretching is expected as a result of the vertical stress decrease. If the stiffness in the reservoir and the surroundings are similar, the corresponding horizontal stress in the overburden is likely to increase during depletion (Geertsma, 1985; Mahi, 2003; Mulders, 2003). In contrast, a relatively stiff overburden as compared with the reservoir may lead to a horizontal stress reduction in the overburden (Morita and Fuh, 2009). Consequently, the stress path parameter κ has opposite polarity in these two cases. The magnitudes of overburden stress changes (stress arching) are promoted by a small aspect ratio of the depleting zone and by a reservoir tilt. The reservoir geometry and the static properties of the subsurface may imply significant lateral variations in the stress paths as a result of stress arching (Sayers and Schutjens, 2007; Fjær *et al.*, 2008).

Several works extend the time-shift analysis beyond the traditional R -factor model, which in several cases build implicitly or explicitly on the idea of the third-order constitutive elastic model proposed by Prioul *et al.* (2004) that is applicable for a VTI medium (Herwanger *et al.*, 2007; Fuck *et al.*, 2009; Rodriguez-Herrera *et al.*, 2015; Kudaraova *et al.*, 2016; MacBeth *et al.*, 2018). The model by Prioul *et al.* (2004) assumes isotropy in the strain sensitivity of the velocities, implying that a single isotropic stress path can determine the full set of third-order parameters for anisotropic rocks. This was applied by Prioul *et al.* (2004) to deduce the three independent third-order parameters from the Kimmeridge shale data of Hornby (1998), by considering only isotropic stress paths. The simplicity and the lack of data that could reveal a lower symmetry in the third-order dynamic correction, may explain the popularity of this model (Fuck *et al.*, 2009). However, the assumption of isotropic strain sensitivity seems not to be consistent with the laboratory data on shales reported by Bakk *et al.* (2018) and Holt *et al.* (2018), indicating that shales exhibit anisotropic strain sensitivities of their anisotropic dynamic stiffness, which also depends on the stress path. Moreover, the magnitude of the R -factor based upon a hydrostatic (isotropic) test may be very misleading for the subsurface, as stress paths are likely to be prone to significant shear-stress changes (Mulders, 2003; De Gennaro *et al.*, 2008; Herwanger and Horne, 2009; Morita and Fuh, 2009). Based upon the model of Prioul *et al.* (2004), the Kimmeridge data of Hornby (1998) yield an R -factor of 35 (Herwanger, 2008). Even though such extreme values are also reported elsewhere (e.g. Staples *et al.*, 2007; De Gennaro *et al.*, 2008), most of the field data seem to exhibit significantly lower R -factors. Our data set strongly

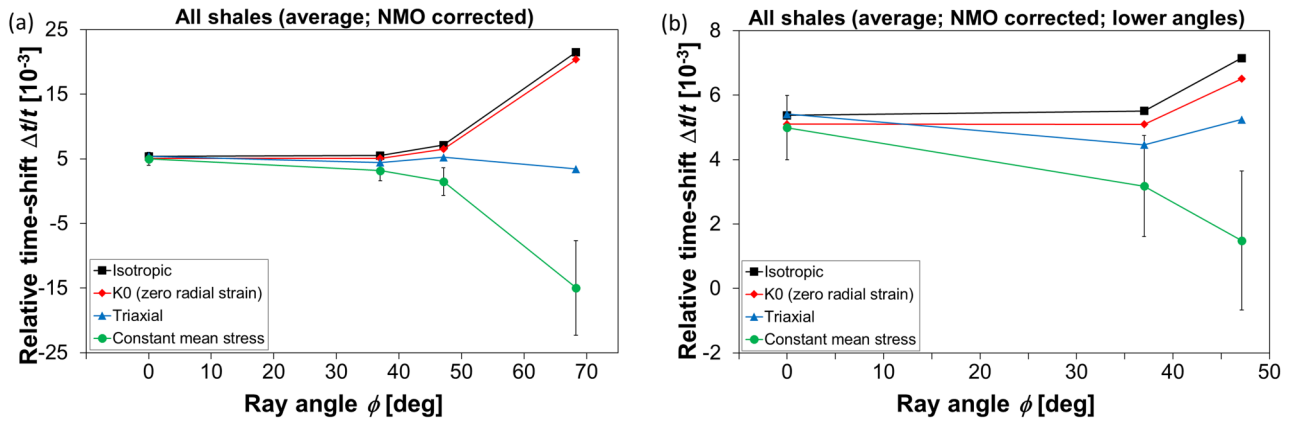


Figure 10 Relative time-shift versus ray angle for the different stress paths corresponding to 5 MPa vertical unloading. The data points are the average values of the three shales and are NMO-corrected according to equation (9). To ease the separation of the stress paths, connection lines between the data points are inserted. (a) The 90° data point is not accessible for NMO-corrected data, even though the horizontal P-wave velocity is measured in the laboratory, since it is not possible to vertically stretch the time-shift for a purely horizontal ray path. (b) The 68° data points are here removed to show that the offset trends of the time-shifts are significant (and nonlinear) also for smaller offsets. The error bars for the constant-mean-stress path correspond to the 95% confidence interval, which are valid for the other stress paths in the same figure (angle for angle).

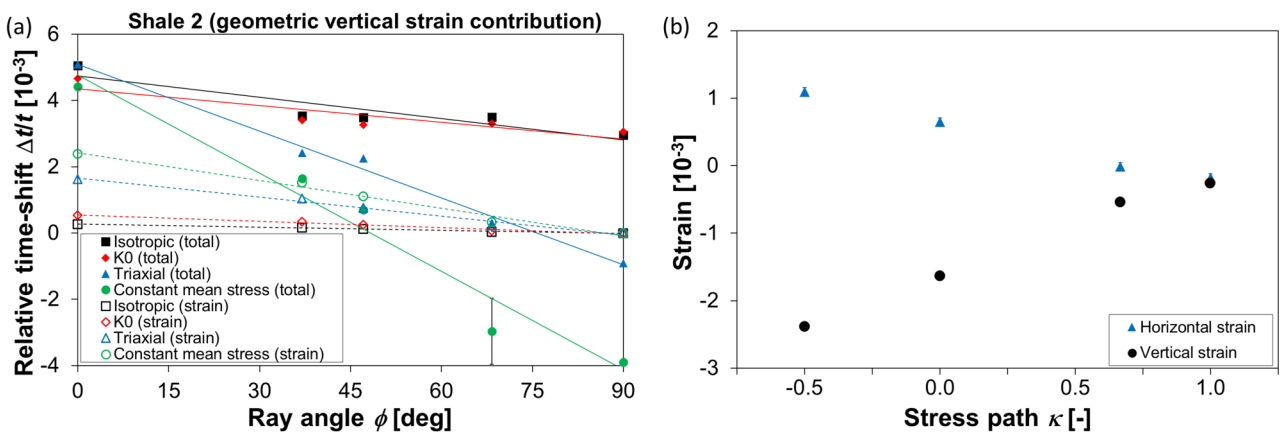


Figure 11 (a) Relative (total) time-shift versus ray angle for the different stress paths for Shale 2 (filled symbols with a solid linear trendline) compared with the explicit geometric contribution from the vertical strain to the time-shift in equation (5) (open symbols with a broken linear trendline). The error bar corresponds to the 95% confidence interval (valid for all data points of the total time-shift). The errors for the time-shifts related to the geometric contribution is limited to the size of the symbols. (b) Horizontal and vertical strains versus stress path for 5 MPa vertical unloading for Shale 2. Zero strain corresponds to the *in situ* reference state. The error is limited to the size of the symbols.

underlines that the *R*-factor is not a constant but is strongly correlated with the stress path with a span for the average values of *R* from 1 for the constant-mean-stress change to 17 for the isotropic stress change (Fig. 7) for our shales. Here it can be mentioned that Hawkins (2008) introduced a heuristic *R*-factor accounting for the stress-induced anisotropy in addition to the common vertical *R*-factor to better match data and implicitly honour the stress path. As an alternative to constitutive models, crack models may also be an adequate choice

providing more intuitive physical understanding (e.g. Sayers and Kachanov, 1995; Fjær, 2006; Shapiro, 2017; MacBeth *et al.*, 2018). The latter may open the possibility for introducing anisotropic crack distributions with anisotropic stress and strain sensitivities, which seem to be important to adequately model the complex static and dynamic behaviour of shales.

The largest offset gradients of the time-shifts in Fig. 8 are observed for the stress paths associated with the most significant shear-stress changes (CMS and triaxial stress paths). To

qualitatively understand this, consider the CMS stress path that has opposite polarities of the vertical and horizontal stress changes, because a vertical unloading is accompanied with a horizontal loading and vice versa. Furthermore, the principal strains will also have opposite polarity in this case, that is, a vertical extension is associated with a horizontal compression and vice versa. Thus, the horizontal and vertical P-waves propagate in directions with opposite stress changes and opposite strains that implies a flip of polarity in the time-shifts at large offsets for the CMS stress path. In contrast, the isotropic stress path is associated with strains of equal polarity in the principal directions, which is reflected in a much smaller offset gradient of the time-shifts. However, because of the static anisotropy, isotropic stress changes imply anisotropic strains, and consequently the dynamic strain sensitivities are likely to be anisotropic for shales for any stress path. This may explain why we also expect some offset gradient of the time-shifts for the isotropic stress path, even in the case of a single, flat and homogeneous reflector. In our laboratory experiments, the whole range of offsets from 0° to 90° is covered. However, field measurements based upon reflection seismic are typically restricted to offsets up to 30° – 40° , depending on the depth of the target and the extent of survey. To mitigate this, complementary seismic data from cross-well or refraction surveys in addition to methods such as full-waveform inversion may turn out to be valuable (Zadeh *et al.*, 2011; Yang *et al.*, 2016). Nevertheless, the offset trends discussed here are also significant even for offsets typical for reflection seismic.

Herwanger *et al.* (2007) show NMO-corrected data from the South-Arne field in the southern North Sea that are associated with a negative offset gradient in the overburden. This is typical for a subsurface with small static stiffness-contrast between the depleting reservoir and the overburden, implying an overburden experiencing close to constant-mean-stress path (Mulders, 2003). The NMO-corrected data in Fig. 10 are qualitatively in line with this, exhibiting a negative offset gradient for the constant-mean-stress path, in contrast to the isotropic stress path and the K_0 stress path. In Fig. 10(b), we show that the offset trends of the time-shifts for the different stress paths are significant and nonlinear also for smaller offsets that are commonly accessible for seismic field surveys. In contrast, a relatively stiffer overburden compared with the reservoir implies a completely different stress path that is closer to isotropic stress changes in the overburden, implying less shear-stress changes as compared with the CMS stress path (De Gennaro *et al.*, 2008; Morita and Fuh, 2009). Such geomechanical constraints will significantly influence the time-shifts. Kudarova *et al.* (2016) present time-shifts from the

Shearwater field in the North Sea where they observe no significant changes (decreases) in time-shifts with increasing offset. Like the data of Herwanger *et al.* (2007), they used NMO-corrected data assuming a constant velocity field for the move-out correction. Seismic pre-stack data are often represented as angle-band stacks to boost the signal. However, NMO corrections may complicate the interpretation and potentially mask essential information from the 4D data set (Hodgson, 2009). In the case of a significant offset dependence of relative time-shifts in 4D field data, it would be beneficial to quantify the offset trend prior the moveout stretch. Then, the moveout stretch could be done by including an appropriate correction for the moveout gradient of time-shift if one uses the baseline line velocity field, which has the same effect as if the correctly updated velocity field was used directly to stretch the data set of the repeated survey. Now, the 4D data set can be stacked to boost the signals. In contrast, if 4D data are just stacked without correcting for any offset gradient, the information that lies in the offset gradient may be lost and the stacked signal becomes blurred.

It should be underlined that a comparison between laboratory data and field data is difficult without specific information about the field and the inversion scheme for the update of the geological model. A 4D field case, due to its complexity, needs to be assessed with respect to the extent and the spatial heterogeneity in the strain field. Intuitively, one would expect that far-offset seismic travel-time shifts are relatively less influenced since the path-length in the effective area that is influenced by the depletion (strain cloud) is relatively shorter as compared with near-offsets. On the other hand, laboratory experiments are much easier to interpret because of relatively homogeneous material properties and well-defined stress and strain fields.

One major benefit with our ultrasonic set-up is that velocities and their stress sensitivities are obtained during a single experiment for each different field shale. This is ideal for the systematic quantification and fundamental understanding of the subsurface. In the field, one faces challenges influencing the offset interpretation as gas clouds in the overburden attenuating the signal, mineral heterogeneities, complex structures and a confined and often irregular overburden strain cloud. Also, the reservoir may be undershot for larger offsets. In the end, all this must be dealt with. Models and correlations based on laboratory experiments can constrain, and thereby ease and improve, the interpretation of seismic data by quantifying the relations between the changes in stresses, strains, velocities and their explicit impact on the time-shifts. With such multistage tests on different rocks that are representative of the relevant

formations (dominating layers), one can build up a database – layer by layer – and make correlations that can generically be used to improve the interpretation of 4D seismic data.

In general, porous sedimentary rocks are dispersive, which potentially implies a significant frequency dependence of velocities (e.g. Spencer, 1981; Batzle *et al.*, 2006). Since the laboratory P-waves we applied in our tests propagate at frequencies in the range of 10^5 – 10^6 Hz and seismic waves propagate typically in the range of 1–100 Hz, dispersion may impact the interpretation of time-lapse data. Laboratory data indicate a larger stress sensitivity for the dynamic stiffness at seismic frequencies as compared with ultrasonic frequencies (Lozovyi, 2018; Szewczyk *et al.*, 2018). However, one should note that these low-frequency experiments are associated with significantly larger uncertainties when compared with ultrasonic measurements. Moreover, it is not clear whether this will bias the interpretation of the offset dependence of time-shifts. Nevertheless, improved low-frequency measurements that are dedicated to study the time-shifts and their offset dependence would be very beneficial.

4 CONCLUSIONS

We present time-shift data for three different overburden field shales, where multidirectional ultrasonic velocities were measured and probed for four different stress paths. The time-shifts are decreasing with increasing ray angles for all shales investigated here, and the constant-mean-stress path exhibits even negative time-shifts for larger angles associated with a significant offset gradient. This contrasts to the isotropic stress path exhibiting a much smaller offset dependence and positive time-shifts for all angles. These data show the importance of calibrated rock physics models for improved 4D seismic inversion. Provided an appropriate rock physics model, pre-stack offset time-shifts from 4D seismic data may quantify the stress changes and strains that are essential for safe and efficient field operations. To fully utilize this potential, such rock physics models and correlations should be accompanied with geomechanical simulations for the inversion of 4D data.

The enhanced time-shift separation between the different stress paths at far offsets (Fig. 8) underlines the potential of seismic pre-stack analysis. In this respect, other methods like seismic refraction tomography or full-waveform inversion may provide additional information about lateral discontinuities in the overburden. Cross-well seismic is also an option, although the potentially extra costs may be a barrier for such deployment. Generally, cost-efficient methods involving better utilization of 4D data are often preferable, in line with the

ongoing digitalization of this industry. Thus, utilizing laboratory data to provide correlations between static and dynamic changes for different offsets may turn out to be a suitable approach in this respect.


ACKNOWLEDGEMENTS

We thank the Research Council of Norway through the PETROMAKS 2 programme, AkerBP, Equinor and Shell in the project *Improved Prediction of Stress and Pore-pressure Changes in the Overburden for Infill Drilling*, and AkerBP, ENGIE, INEOS and Total in the project *Shale Rock Physics: Improved Seismic Monitoring for Increased Recovery* for funding (grants 294369 and 234074, respectively). We also thank Jørn Stenebråten and Eyvind F. Sønstebø for conducting the multistage shale tests at the SINTEF Formation Physics Laboratory. The discussions with Idar Larsen on the signal analysis are highly appreciated. We also thank the Editor (Noalwenn Dubos-Sallee) and the two anonymous reviewers for their comments and suggestions on this paper.


DATA AVAILABILITY STATEMENT


Restrictions apply to the availability of these data that support the results of this study, which were generated under the projects ‘*Improved prediction of stress and pore-pressure changes in the overburden for infill drilling*’ and ‘*Shale Rock Physics: Improved Seismic Monitoring for Increased Recovery*’. Data are available from SINTEF AS, by its research institute SINTEF Industry, subject to the permissions of the owners of the data.

ORCID

Audun Bakk  <https://orcid.org/0000-0003-0581-6909>

Rune M. Holt  <https://orcid.org/0000-0003-1763-7836>

Bastien Dupuy  <https://orcid.org/0000-0002-1712-5972>

Anouar Romdhane  <https://orcid.org/0000-0002-0989-9898>

REFERENCES

- Angus, D.A., Dutko, M., Kristiansen, T.G., Fisher, Q.J., Kendall, J.-M., Baird, A.F., Verdon, J.P. *et al.* (2015) Integrated hydro-mechanical and seismic modelling of the Valhall reservoir: a case study of predicting subsidence, AVOA and microseismicity. *Geomechanics for Energy and the Environment*, **2**, 32–44.
- Bakk, A., Stenebråten, J.F., Lozovyi, S., Bauer, A., Sønstebø, E.F., Fjær, E., Bhuiyan, M.H. *et al.* (2018) Static and dynamic characterization

- of a deep overburden shale. *80th EAGE Conference & Exhibition*, Copenhagen, Denmark, Expanded Abstracts, We-A11-09. <https://doi.org/10.3997/2214-4609.201801020>.
- Bathija, A.P., Batzle, M.L. and Prasad, M. (2009) An experimental study of the dilation factor. *Geophysics*, **74**(4), E181–E191.
- Batzle, M.L., Han, D.-H. and Hofmann, R. (2006) Fluid mobility and frequency-dependent seismic velocity – direct measurements. *Geophysics*, **71**(1), N1–N9.
- Calvert, M.A., Cherrett, A.J., Micksch, U., Bourgeois, F.G. and Calvert, A.S. (2018) New time lapse seismic attribute linking 4D and geomechanics. *80th EAGE Conference & Exhibition*, Copenhagen, Denmark, Expanded Abstracts, Tu-A15-12. <https://doi.org/10.3997/2214-4609.201800698>.
- De Gennaro, S., Onaisi, A., Grandi, A., Ben-Brahim, L. and Neillo, V. (2008) 4D reservoir geomechanics: a case study from the HP/HT reservoirs of the Elgin and Franklin fields. *First Break*, **26**, 53–59.
- Dillen, M.W.P., Cruts, H.M.A., Groenenboom, J., Fokkema, J.T. and Duijndam, A.J.W. (1999) Ultrasonic velocity and shear-wave splitting behaviour of a Colton sandstone under a changing triaxial stress. *Geophysics*, **64**, 1603–1607.
- Ditlevsen, F., Bourgeois, F. and Calvert, M. (2018) Handling wellbore instability in overburden Tertiary shales. *80th Annual EAGE Meeting*, Copenhagen, Denmark, Expanded Abstracts, Tu-C-07. <https://doi.org/10.3997/2214-4609.201800721>.
- Dudley, J.W., Brignoli, M., Crawford, B.R., Ewy, R.T., Love, D.K., McLennan, J.D., Ramos, G.G. *et al.* (2016) ISRM suggested method for uniaxial-strain compressibility testing for reservoir geomechanics. *Rock Mechanics and Rock Engineering*, **49**, 4153–4178.
- Fjær, E. (2006) Modeling the stress dependence of elastic wave velocities in soft rocks. *41st US Rock Mechanics/Geomechanics Symposium*, Golden, USA, ARMA 06-1070. <https://www.onepetro.org/conference-paper/ARMA-06-1070>.
- Fjær, E., Holt, R.M., Horsrud, P., Raaen, A.M. and Risnes, R. (2008) *Petroleum Related Rock Mechanics*. 2nd edn. Elsevier Science. <https://www.elsevier.com/books/petroleum-related-rock-mechanics/fjar/978-0-444-50260-5>.
- Fuck, R.F., Bakulin, A. and Tsvankin, I. (2009) Theory of traveltimes shifts around compacting reservoirs: 3D solutions for heterogeneous anisotropic media. *Geophysics*, **74**(1), D25–D36.
- Fuck, R.F. and Tsvankin, I. (2009) Analysis of the symmetry of a stressed medium using nonlinear elasticity. *Geophysics*, **74**(5), WB79–WB87.
- Geertsma, J. (1985) Some rock-mechanical aspects of oil and gas well completions. *Society of Petroleum Engineers Journal*, **25**, 848–856.
- Grechka, V. and Tsvankin, I. (1998) Feasibility of nonhyperbolic moveout inversion in transversely isotropic media. *Geophysics*, **63**, 957–969.
- Guilbot, J. and Smith, B. (2002) 4-D constrained depth conversion for reservoir compaction estimation: application to Ekofisk field. *The Leading Edge*, **21**, 302–308.
- Hall, S.A., MacBeth, C., Barkved, O.I. and Wild, P. (2002) Time-lapse seismic monitoring of compaction and subsidence at Valhall through cross-matching and interpreted warping of 3D streamer and OBC data. *72nd SEG Annual Meeting*, Salt Lake City, USA, Expanded Abstracts, 1696–1699. <https://doi.org/10.1190/1.1817004>.
- Hatchell, P.J., van denBeukel, A., Molenaar, M.M., Maron, K.P., Kenter, C.J., Stammeijer, J.G.F., van derVelde, J.J. *et al.* (2003) Whole Earth 4D: reservoir monitoring geomechanics. *73rd SEG Annual Meeting*, Dallas, USA, Expanded Abstracts, 1330–1333. <https://doi.org/10.1190/1.1817532>.
- Hatchell, P. and Bourne, S. (2005) Rocks under strain: strain-induced time-lapse time shifts are observed for depleting reservoirs. *The Leading Edge*, **24**, 1222–1225.
- Hawkins, K. (2008) Defining the extent of the compacting Elgin reservoir by measuring stress-induced anisotropy. *First Break*, **26**, 81–88.
- Hawkins, K., Harris, P. and Conroy, G. (2006) Estimating production-induced stress changes from 4D finite offset timeshifts. *68th EAGE Conference & Exhibition*, Vienna, Austria, Expanded Abstracts, P196. <https://doi.org/10.3997/2214-4609.201402276>.
- Hawkins, K., Howe, S., Hollingworth, S., Conroy, G., Ben-Brahim, L., Tindle, C., Taylor, N. *et al.* (2007) Geomechanical stresses from 4D timeshifts measured around the depleting Franklin and Elgin reservoirs. *77th SEG Annual Meeting*, San Antonio, USA, Expanded Abstracts, 2862–2866. <https://doi.org/10.1190/1.2793061>.
- Herwanger, J. (2008) R we there yet? *70th EAGE Conference & Exhibition*, Rome, Italy, Expanded Abstracts, I029. <https://doi.org/10.3997/2214-4609.20147816>.
- Herwanger, J.V. and Horne, S.A. (2009) Linking reservoir geomechanics and time-lapse seismics: predicting anisotropic velocity changes and seismic attributes. *Geophysics*, **74**(4), W13–W33.
- Herwanger, J., Palmer, E. and Schiøtt, C.R. (2007) Anisotropic velocity changes in seismic time-lapse data. *77th SEG Annual Meeting*, San Antonio, USA, Expanded Abstracts, 2883–2887. <https://doi.org/10.1190/1.2793065>.
- Hodgson, N. (2009) Inversion for reservoir pressure change using overburden strain measurements determined from 4D seismic. PhD thesis, Heriot-Watt University, Edinburgh, UK. <https://www.ros.hw.ac.uk/handle/10399/2320>.
- Holt, R.M. (2016) Bounds of elastic parameters characterizing transversely isotropic media: application to shales. *Geophysics*, **81**(5), C243–C252.
- Holt, R.M., Bauer, A. and Bakk, A. (2018) Stress-path-dependent velocities in shales: impact on 4D seismic interpretation. *Geophysics*, **83**(6), MR353–MR367.
- Holt, R.M., Bhuiyan, M.H., Kolstø, M.I., Bakk, A., Stenebråten, J.F. and Fjær, E. (2011) Stress-induced versus lithological anisotropy in compacted claystones and soft shales. *The Leading Edge*, **30**, 312–317.
- Hornby, B.E. (1998) Experimental laboratory determination of the dynamic elastic properties of wet, drained shales. *Journal of Geophysical Research*, **103**, 29945–29964.
- Horsrud, P., Sønstebo, E.F. and Bøe, R. (1998) Mechanical and petrophysical properties of North Sea shales. *International Journal of Rock Mechanics and Mining Sciences*, **35**, 1009–1020.
- Johnson, P.A. and Rasolofosaon, P.N.J. (1996) Nonlinear elasticity and stress-induced anisotropy in rock. *Journal of Geophysical Research*, **101**, 3113–3124.
- Jones, L.E.A. and Wang, H.F. (1981) Ultrasonic velocities in Cretaceous shales from the Williston Basin. *Geophysics*, **46**, 288–297.

- Kenter, C.J., Van den Beukel, A.C., Hatchell, P.J., Maron, K.P., Moleenaar, M.M. and Stammeijer, J.G.F. (2004) Evaluation of reservoir characteristics from time shifts in the overburden. *Gulf Rocks 2004; 6th North America Rock Mechanics Symposium (NARMS)*, Paper, ARMA/NARMS 04-627. <https://www.onepetro.org/conference-paper/ARMA-04-627>.
- Kudrova, A., Hatchell, P., Brain, J. and MacBeth, C. (2016) Offset-dependence of production-related 4D time-shifts: real data examples and modelling. *86th SEG Annual Meeting*, Dallas, USA, Expanded Abstracts, 5395–5399. <https://doi.org/10.1190/segam2016-13611549.1>.
- Landrø, M. and Janssen, R. (2002) Estimating compaction and velocity changes from time-lapse near and far offset stacks. *64th EAGE Conference & Exhibition, Florence, Italy, Extended Abstracts*, P036. <https://doi.org/10.3997/2214-4609-pdb.5.P036>.
- Landrø, M. and Stammeijer, J. (2004) Quantitative estimation of compaction and velocity changes using 4D impedance and traveltimes changes. *Geophysics*, **69**, 949–957.
- Lavrov, A. (2016) Dynamics of stresses and fractures in reservoir and cap rock under production and injection. *Energy Procedia*, **86**, 381–390.
- Lozovyi, S. (2018) Seismic dispersion and the relation between static and dynamic Stiffness of shales. PhD thesis, NTNU, Norway. <https://ntnuopen.ntnu.no/ntnu-xmlui/handle/11250/2564704>.
- Lozovyi, S., Bauer, A., Giger, S. and Chakraborty, S. (2018) Static vs. dynamic stiffness of shales: frequency and stress effects. *52nd US Rock Mechanics/Geomechanics Symposium*, Golden, USA, ARMA 18-257. https://www.researchgate.net/publication/332809564_Static_vs_Dynamic_Stiffness_of_Shales_Frequency_and_Stress_Effects.
- MacBeth, C., Kudrova, A. and Hatchell, P.J. (2018) A semi-empirical model of strain sensitivity for 4D seismic interpretation. *Geophysical Prospecting*, **66**, 1327–1348.
- MacBeth, C., Mangriotis, M.-D. and Amini, H. (2019) Post-stack 4D seismic time-shifts: interpretation and evaluation. *Geophysical Prospecting*, **67**, 3–31.
- Mahi, A. (2003) Stress path of depleting reservoirs. MSc thesis, NTNU, Norway.
- Morita, N. and Fuh, G.-F. (2009) Parametric analysis of stress reduction in the caprock above compacting reservoirs. *SPE Drilling & Completion*, **24**, 659–670.
- Mulders, F.M.M. (2003) Modeling of stress development and fault slip in and around a producing gas reservoir. PhD thesis, TU Delft, the Netherlands. <https://repository.tudelft.nl/islandora/object/uuid%3Abe742135-10d7-4d69-bdee-f808b5926065>.
- Pervukhina, M., Dewhurst, D., Gurevich, B., Kuila, U., Siggins, T., Raven, M. and Bolás, H.M.N. (2008) Stress-dependent elastic properties of shales: measurement and modelling. *The Leading Edge*, **27**, 772–779.
- Prioul, R., Bakulin, A. and Bakulin, V. (2004) Nonlinear rock physics model for estimation of 3D subsurface stress in anisotropic formations: theory and laboratory verification. *Geophysics*, **69**, 415–425.
- Rickett, J., Duranti, L., Hudson, T., Regel, B. and Hodgson, N. (2007) 4D time strain and the seismic signature of geomechanical compaction at Genesis. *The Leading Edge*, **26**, 644–647.
- Rodriguez-Herrera, A., Koutsabeloulis, N., Onaisi, A., Fiore, J. and Selva, F. (2015) Stress-induced signatures in 4D seismic data: evidence of overburden stress arching. 85th SEG Annual Meeting, New Orleans, USA, Expanded Abstracts, 5368–5372. <https://doi.org/10.1190/segam2015-5900945.1>.
- Røste, T., Dybvik, O.P. and Søreide, O.K. (2015) Overburden 4D time shifts induced by reservoir compaction at Snorre field. *The Leading Edge*, **34**, 1366–1374.
- Røste, T. and Ke, G. (2017) Overburden 4D time shifts – indicating undrained areas and fault transmissibility in the reservoir. *The Leading Edge*, **36**, 423–430.
- Røste, T., Stovas, A. and Landrø, M. (2005) Estimation of layer thickness and velocity changes using 4D prestack seismic data. *67th EAGE Conference & Exhibition*, Madrid, Spain, Extended Abstracts, C010. <https://doi.org/10.1190/1.2335657>.
- Sarout, J., Esteban, L., Delle Piane, C., Maney, B. and Dewhurst, D.N. (2014) Elastic anisotropy of opalinus clay under variable saturation and triaxial stress. *Geophysical Journal International*, **198**, 1662–1682.
- Sayers, C.M. and Kachanov, M. (1995) Microcrack-induced elastic wave anisotropy of brittle rocks. *Journal of Geophysical Research*, **100**, 4149–4156.
- Sayers, C.M. and Schutjens, P.M.T.M. (2007) An introduction to reservoir geomechanics. *The Leading Edge*, **26**, 597–601.
- Shapiro, S.A. (2017) Stress impact on elastic anisotropy of triclinic porous and fractured rocks. *Journal of Geophysical Research*, **122**, 2034–2053.
- Skempton, A.W. (1954) The pore-pressure coefficients *A* and *B*. *Géotechnique*, **4**, 143–147.
- Spencer, J.W. (1981) Stress relaxations at low frequencies in fluid-saturated rocks: attenuation and modulus dispersion. *Journal of Geophysical Research*, **86**, 1803–1812.
- Staples, R., Ita, J., Burrell, R. and Nash, R. (2007) Monitoring pressure depletion and improving geomechanical models of the Shearwater field using 4D seismic. *The Leading Edge*, **26**, 636–642.
- Szewczyk, D., Bauer, A. and Holt, R.M. (2018) Stress-dependent elastic properties of shales—laboratory experiments at seismic and ultrasonic frequencies. *Geophysical Journal International*, **212**, 189–210.
- Tempone, P., Landrø, M., Fjær, E. and Inoue, N. (2009) Effects on time-lapse seismic of a hard rock layer beneath a compacting reservoir. *SPE EUROPEC/71st EAGE Conference & Exhibition*, Amsterdam, the Netherlands, Expanded Abstracts, SPE 121081. <https://www.onepetro.org/conference-paper/SPE-121081-MS>.
- Thomsen, L. (1986) Weak elastic anisotropy. *Geophysics*, **51**, 1954–1966.
- Thurston, R.N. and Brugger, K. (1964) Third-order elastic constants and the velocity of small amplitude elastic waves in homogeneously stressed media. *Physical Review*, **133**(6A), A1604–A1610.
- Toomey, A., Fowler, S., van Gestel, J.P., Kristiansen, T.G., Brew, G., Horiuchi, M. and Levine, R. (2017) Stress arching and its impact on 4D seismic amplitudes and traveltimes. *The Leading Edge*, **36**, 895–901.
- Yang, D., Liu, F., Morton, S., Malcolm, A. and Fehler, M. (2016) Time-lapse full-waveform inversion with ocean-bottom-cable data: application on Valhall field. *Geophysics*, **81**(4), R225–R235.

- Yuan, R.S., Schutjens, P.M.T.M., Bourgeois, F.G. and Calvert, M.A. (2018) Fault slip or bed-parallel shear? – a multi-scenario modeling approach to investigating well deformation in the deep overburden of a compacting reservoir in the North Sea. *52nd US Rock Mechanics/Geomechanics Symposium*, Seattle, USA, ARMA 18-610. <https://www.onepetro.org/conference-paper/ARMA-2018-610>.
- Zadeh, H.M, Landrø, M. and Barkved, O.I. (2011) Long-offset time-lapse seismic: tested on the Valhall LoFS data. *Geophysics*, 76(2), O1–O13.
- Zoback, M.D. and Zinke, J.C. (2002) Production-induced normal faulting in the Valhall and Ekofisk oil fields. *Pure and Applied Geophysics*, 159, 403–420.